NANOSYSTEMS: PHYSICS, CHEMISTRY, MATHEMATICS, 2014, 5 (3), P. 441–449

EFFECT OF CALCINATION TEMPERATURE ON THE STRUCTURAL AND OPTICAL PROPERTIES OF NICKEL OXIDE NANOPARTICLES

P. A. Sheena[1], K. P. Priyanka[2], N. Aloysius Sabu[2], Boby Sabu[2], Thomas Varghese[2,*]

[1]M. E. S. Asmabi College, P. Vemballur - 680671, Kerala, India

[2]Nanoscience Research Centre (NSRC), Department of Physics, Nirmala College, Muvattupuzha - 686 661, Kerala, India

[*]nanoncm@gmail.com

PACS 78.67.Bf, 81.16.Be, 81.07.Bc

Herein, we report the effect of calcination on the structural and optical properties of nanocrystalline NiO. NiO nanoparticles were synthesized by chemical precipitation method using nickel nitrate hexahydrate and ammonium carbonate. Thermogravimetric analysis was done to determine the thermal behavior of the precursor. The samples were characterized by X-ray diffraction (XRD), energy dispersive X-ray analysis (EDAX), high resolution transmission electron microscopy (HRTEM), Fourier transform infrared spectroscopy (FTIR), UV-visible and photoluminescence (PL) spectroscopy. Crystallite size and lattice strain on peak broadening of NiO nanoparticles have been studied using Williamson–Hall (WH) analysis. Significant modifications were observed in the crystallite size, absorption spectra and photoluminescence intensity due to calcination. The desired structural and optical properties of NiO nanoparticle make it as a promising material for optoelectronic applications.

Keywords: nickel oxide nanoparticles, chemical precipitation, calcination, crystallite size, optical band gap.

Received: 8 May 2014
Revised: 24 May 2014

1. Introduction

In recent years nanocrystalline transition metal oxides have attracted extensive interest due to their different potential applications. Out of these, Nickel oxide (NiO) is an attractive material due to its chemical stability. NiO has a wide intrinsic band gap of $\sim$ 3.6 eV. It shows interesting optical, electrical and magnetic properties [1, 2]. It is a promising candidate for wide range of applications such as smart windows, gas sensors [3], catalysts [4-6], anode material in Li ion batteries and nanoscale optoelectronic devices such as electro chromic display [7, 8]. As an ion storage material, NiO semiconductor becomes a motivating topic in the new era of research. These applications can be enhanced by decreasing the particle size and hence a precise control of the size and distribution in the nanometer region is required.

Various techniques have been adopted for the synthesis of NiO nanostructures such as sol-gel [9-12], co-precipitation [12], hydrothermal [13], solvo-thermal [14] and chemical precipitation [6, 15]. In the present study, we have prepared NiO nanoparticles using the chemical precipitation route which can yield high purity products at low cost starting from easily available materials. Synthesized NiO nanoparticles have been characterized by XRD, EDAX, TEM, FTIR spectroscopy, UV-visible and PL spectroscopy.

2. Experimental details

Nickel nitrate hexahydrate ($Ni(NO_3)_26H_2O$) (99.8%, Merck) and ammonium carbonate ($(NH_4)_2CO_3$)(99.9%, Merck) were used without further purification for the synthesis of NiO. Distilled water was used in all synthesis procedures.

2.1. Preparation of the sample

Nanocrystalline NiO samples were prepared by reacting aqueous solutions of nickel nitrate hexahydrate and ammonium carbonate (0.1M each) under stirring. The green precipitate formed was washed with distilled water several times to remove the unreacted salts, and dried in a hot air oven at 70°C for 20 h. The precursor obtained was calcined in a muffle furnace at different temperatures, ranging from 400–600°C for 2 hours, which resulted in a black solid mass. NiO samples calcined at 400°C, 500°C and 600°C are denoted as S1, S2 and S3 respectively.

2.2. Characterization techniques

Thermogravimetric (TG) analysis of the precursor was carried out using a Perkin Elmer, Diamond instrument with a heating rate of 10.00°C/min. The structural characterization of the samples were done by X-ray powder diffraction using Bruker D8 Advance X-ray diffractometer ($\lambda = 1.5406$ Å, step size = 0.020° and dwell time = 31.2 s) with CuKα radiation in 2θ range from 20 to 80°. EDAX spectrum was obtained on a JEOL Model JED–2300 equipment with an accelerating voltage of 30 kV. TEM and HRTEM images were recorded on a JEOI–2010 at an accelerating voltage of 200 kV. Fourier transform infrared spectra of the samples were recorded using Thermo Nicolet, Avatar 370 instrument. Shimadzu 2600/2700 UV–Visible spectrophotometer was used to record the optical absorption spectra of the samples in a wavelength range of 200 to 600 nm. Photoluminescence spectra were measured over wavelengths ranging from 250–650 nm at room temperature by a Fluoromax3 spectrophotometer.

3. Results and discussion

3.1. Thermogravimetric analysis

Fig. 1 shows the thermal decomposition result of the precursor from the ambient temperature to 700°C using both the thermogravimetric and the differential thermogravimetric (DTG) curves. The TG curve indicates that the weight loss of the precursor occurred from 50°C to 350°C. This suggests that the precursor decomposed completely at 350°C to become nickel oxide [10, 16]. Therefore the choice of suitable calcination temperature is highly dependent on the results of TG analysis. Two distinct intervals of weight loss were observed in the TG curve, accompanied by two peaks of weight loss rate in the DTG curve. The first peak located around 100°C might be attributed to the thermal dehydration of the precursor and the evaporation of physically adsorbed impurities. The second peak near 300°C may be related to the decomposition of nickel carbonate. Based on the results of TGA, a temperature of 400°C was chosen to ensure the complete decomposition of the precursor to form nickel oxide.

3.2. XRD analysis

The phase composition, purity and structure of the samples were examined using XRD. Fig. 2 depicts the XRD patterns of the samples calcined at different temperatures. Well defined diffraction peaks are observed in the figure corresponding to (111), (200), (220),

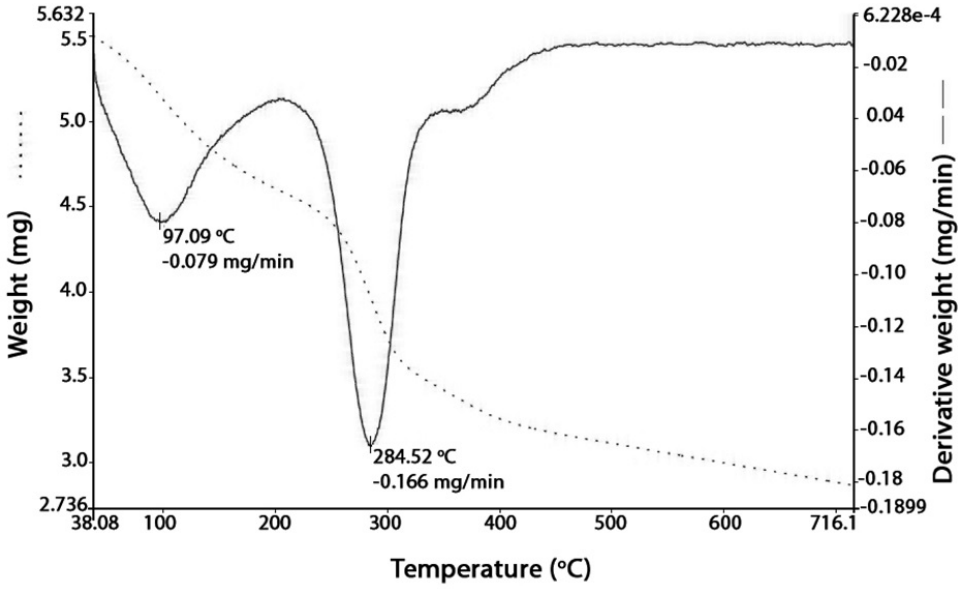

FIG. 1. TG/DTG curve for NiO nanoparticles

(311) and (222) planes of cubic NiO crystals, which are in accordance with the standard spectrum (JCPDS, No.73-1519) [11]. From the analysis of positions and relative intensities of the diffracted peaks, the presence of single phase cubic structure of NiO with a space group Fm3m is confirmed. Lattice constants calculated from XRD data are 0.4180 nm, 0.4176 nm and 0.4171 nm respectively, for samples S1, S2 and S3 which are in good agreement with the reported data [17].

Fig. 2 shows that the diffraction peaks become intense and their full width at half maximum (FWHM) gradually decreases with increasing calcination temperatures. The reason is that at higher calcination temperatures, the formed crystallites are larger in size, which can be attributed to the thermally promoted crystallite growth.

The crystallite sizes of all samples were calculated from the line broadening of the diffraction peaks using Scherrer's formula [18]. The crystallite size was found to increase with an increase in the calcination temperature. Williamson- Hall analysis was carried out to calculate the contributions of size and micro-diffraction to XRD line broadening. The W-H equation [19-21] is given by,

$$\beta \cos\theta = k\lambda/D + 4\varepsilon \sin\theta. \tag{1}$$

The results are presented in table 1. The very small micro-diffraction values for all the samples lead to the close agreement between the crystallite sizes estimated from Scherrer's equation and W-H analysis. The presence of O vacancies, structural imperfections and surface defects in NiO nanoparticles can introduce micro-diffraction that results in the broadening of XRD peaks [22, 23]. It is found that the micro-diffraction for NiO calcined at 400°C has large value, which decreases with increase in calcination temperature. This occurs because defects like dislocations, edges or cuts are probably removed during the calcination process [22].

3.3. Energy dispersive X- ray analysis

Nickel (II) oxide is generally known as a non-stoichiometric compound ($Ni_{1-x}O$) with color varying from gray to black. EDAX analysis was carried out to know the presence of

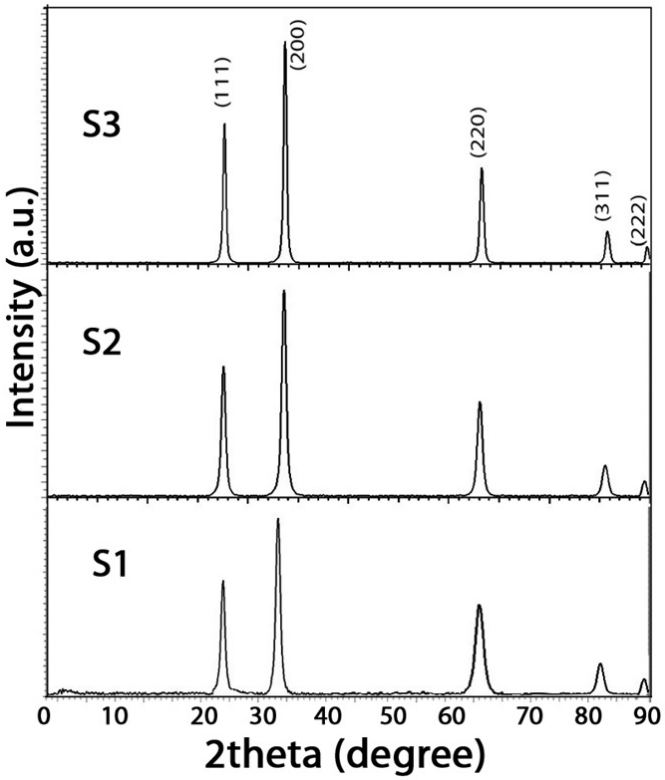

FIG. 2. XRD patterns of the NiO nanoparticle samples

TABLE 1. Geometric parameters of NiO nanoparticle from XRD spectra

Sample	Particle size (nm) Sherrer's equation	W-H method	
		Particle size (nm)	Microstrain ($*10^{-3}$)
S1	9.82±0.196	10.83±0.217	6.67±0.13
S2	16.84±0.337	16.91±0.338	0.65±0.013
S3	23.54±0.47	26.16±0.523	0.1±0.002

nickel oxide in the sample. The EDAX pattern (Fig. 3) of the sample shows the presence of nickel and oxygen. The mass percentage and the atom percentage of the prepared sample are given in table 2. EDAX confirmed that the NiO sample contains nickel and oxygen with a molecular ratio of 1 : 1, with no trace of any other materials.

TABLE 2. EDAX data for NiO nanoparticles

Elements	keV	Mass %	Atom %
O K	0.525	9.3±0.186	27.34±0.547
Ni K	7.471	90.7±1.814	72.66±1.453
Total		100	100

3.4. TEM analysis

In order to reveal the morphology and size of the synthesized products, typical TEM and HRTEM images have been recorded, as shown in Fig. 4. Fig. 4(a) shows the TEM

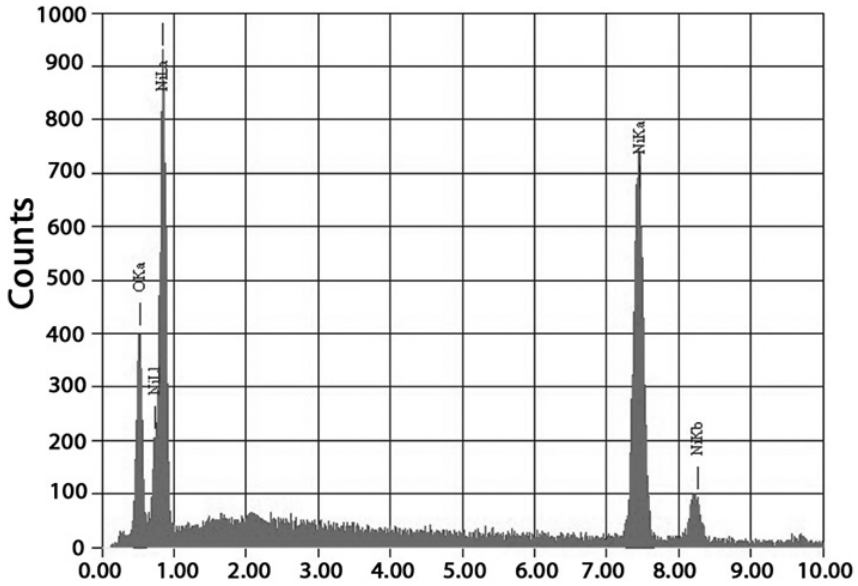

FIG. 3. EDAX pattern of NiO nanoparticles

bright field images of NiO nanoparticles calcined at 400°C. It can be clearly observed that the synthesized product consisted of nearly cube shaped particles with size around 13 nm. However, average crystallite sizes obtained from Scherrer's formula and W–H analysis show a slight decrease from that of TEM images, because of the difference in averaging particle size distribution. The lattice fringes can be clearly seen from the HRTEM image (Fig. 4(b)), in which inter planar distance is determined to be about 0.21 nm, which is consistent with the d spacing of (200) of cubic NiO. From HRTEM image the unidirectional fringe patterns are clearly observed, which indicates single crystalline nature of NiO nanoparticle.

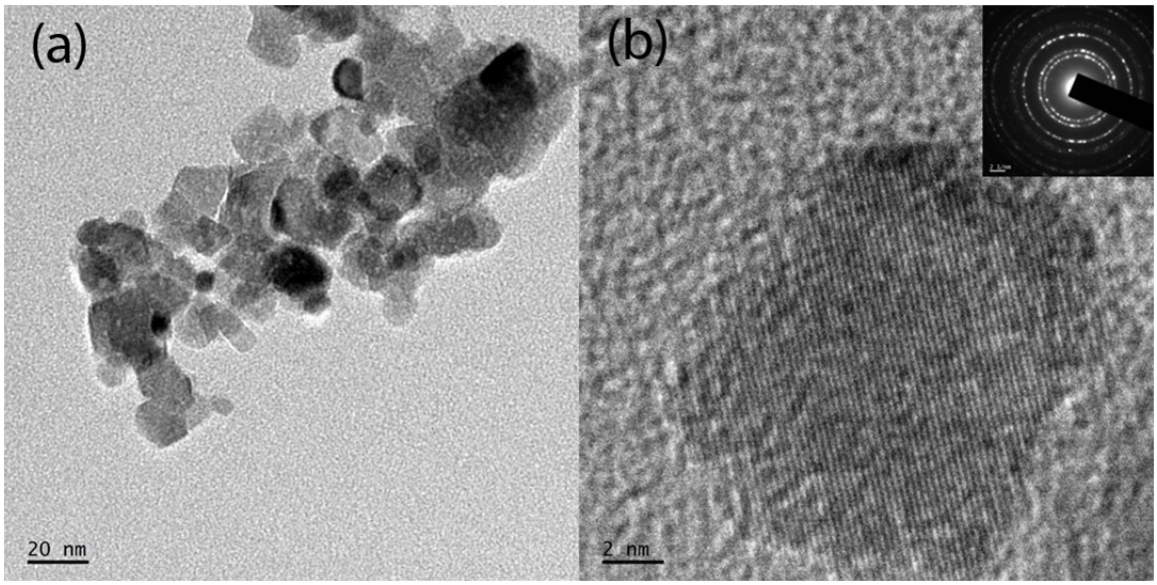

FIG. 4. TEM images of NiO nanoparticles calcined at 400°C

Selected area electron diffraction pattern (SAED) originated from the NiO nanoparticles is shown in the inset of Fig. 4 (b). The appearance of strong diffraction spots rather

than diffraction rings confirmed the formation of single crystalline cubic nickel oxide. Size distribution and abundance of NiO nanoparticles is plotted in histogram shown in Fig. 5.

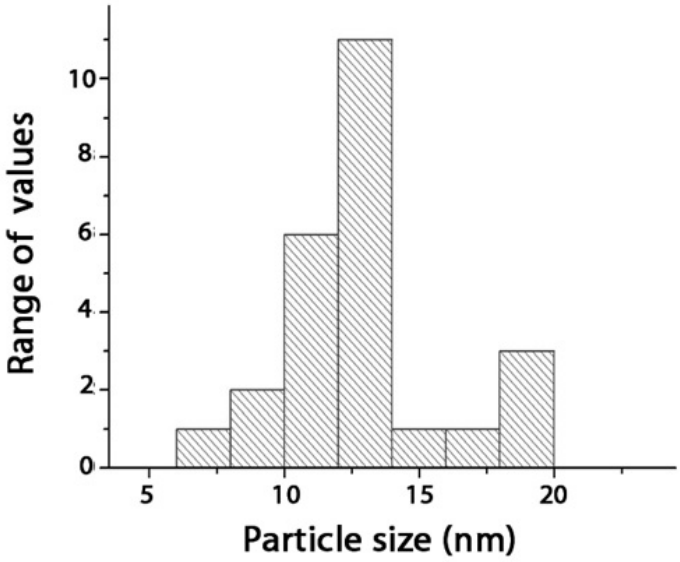

FIG. 5. Size distribution of NiO nanoparticles

3.5. FTIR analysis

The FTIR spectra of the samples calcined ed at 400°C and 500°C are shown in Fig. 6. The spectrum has several significant absorption peaks recorded in the range of 4000 cm^{-1} to 400 cm^{-1}. The broad absorption band centered at 3450 cm^{-1} is assigned to O–H stretching vibrations and the band at 1630 cm^{-1} is attributable to H–O–H bending vibration mode. These indicate the presence of traces of water in the sample. The broad absorption band in the region 430–490 cm^{-1} is assigned to Ni–O stretching vibration mode [14]. The broadness of the band indicates the nanocrystalline nature of the samples.

3.6. UV - Vis studies

Fig. 7 shows UV-visible absorption spectra and $(\alpha h\nu)^2$ versus energy plot for NiO nanoparticles samples. It can be seen (Fig. 7 (a)) that there is an exponential decrease in the intensity of absorption with increase in wavelength. This behavior is typical for many semiconductors and can occur due to various reasons like internal electric fields within the crystal, deformation of lattice due to strain caused by imperfection and inelastic scattering of charge carriers by phonons [9]. It can be seen from Fig. 7 (a) that the absorption edge corresponding to samples S1, S2 and S3 are at 365, 375 and 415 nm respectively. Small blue shift was exhibited by samples S1 and S2 because of their small particle sizes.

Optical band gap energy values obtained from Fig. 7 (b) are 3.385, 3.30, and 3.18 eV respectively for the samples S1, S2 and S3. The optical band gap of NiO in the present study is lower than the bulk value (3.65 eV). This may be due to the chemical defects or vacancies present in the crystal generating new energy level to reduce the band gap energy. However, the band gap is found to decrease with an increase in the calcination temperature due to the crystallite growth.

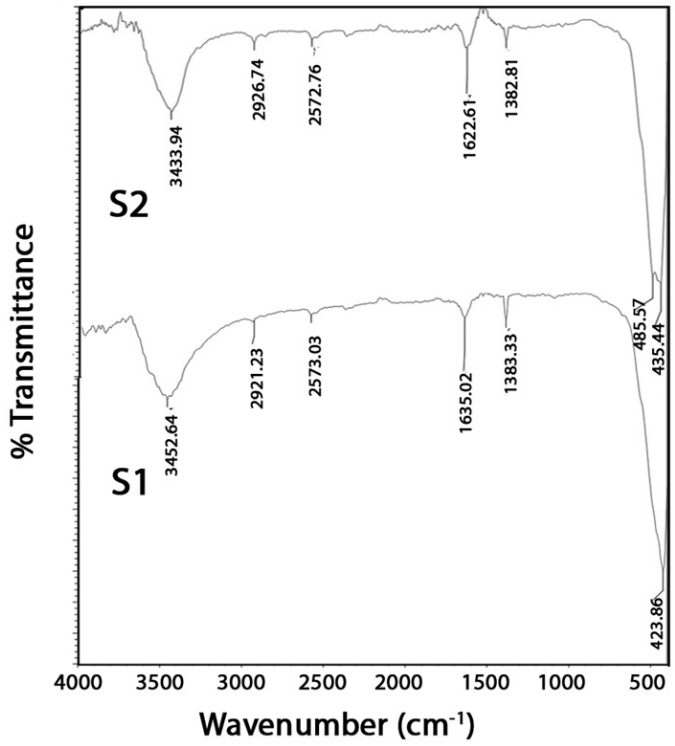

FIG. 6. FTIR spectra of NiO nanoparticle samples

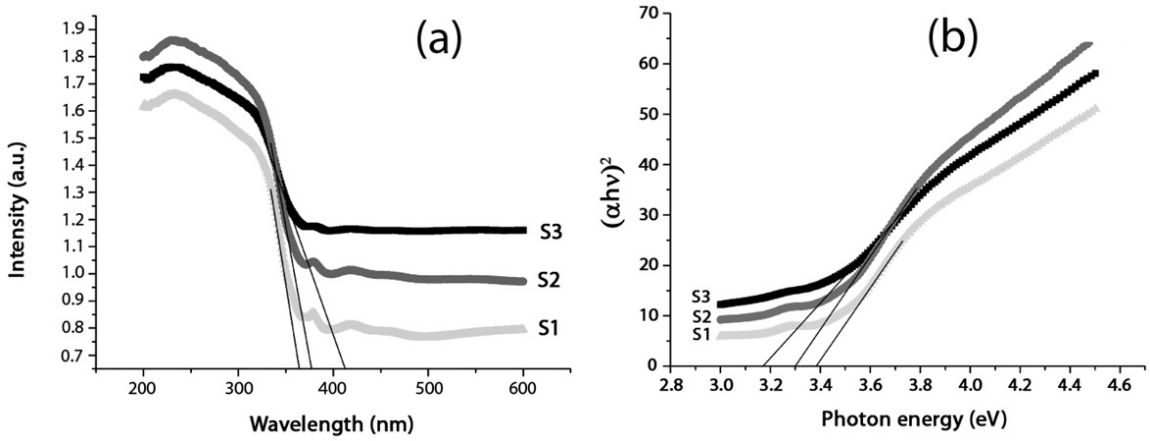

FIG. 7. (a) UV-Visible absorbance specta and (b) $(\alpha h\upsilon)^2$ vs energy plot for NiO samples

3.7. PL studies

Room temperature photoluminescence emission spectra of NiO nanoparticle samples calcined at different temperatures are shown in Fig. 8. NiO nanoparticles exhibit a strong and wide peak in the 350 to 425 nm range with an excited wavelength of 280 nm. The figure shows two obvious PL peaks at about 448 and 466 nm along with some shoulder emission peaks at 370, 380, 396, 410, 481 and 490 nm. The origin of photoluminescence peaks is attributed to electronic transitions involving $3d^8$ electrons of the Ni^{2+} ions [14].

The broad peak in PL spectra corresponds to the direct recombination between electrons in the conduction band and holes in the valence band. It is found that the PL intensity

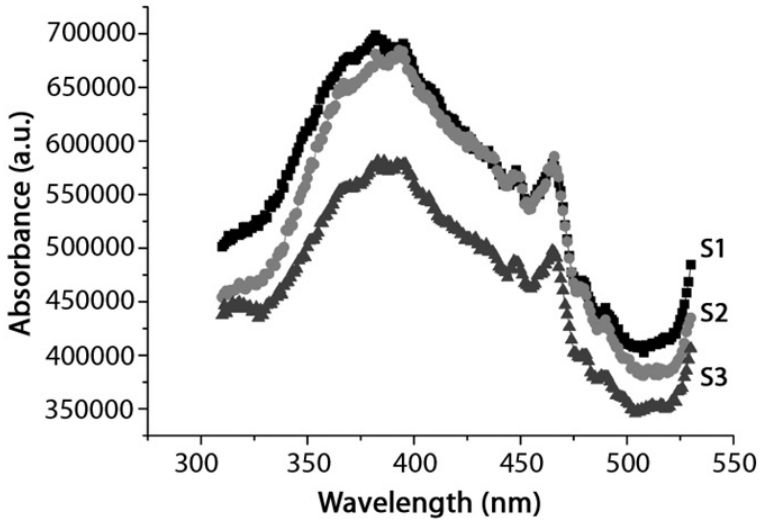

FIG. 8. Room temperature PL spectra for NiO samples

remains the same for samples S1 and S2. However, there was a decrease in intensity for the sample S3. If the size of particle is smaller, oxygen vacancy content is larger, and absorption over UV and visible range increases. Hence, samples S1 and S2 have higher chance of exciton occurrence, which in turn cause stronger PL signal. Moreover, calcination can result in decreased PL intensity due to crystal growth.

4. Conclusions

Nanostructured NiO particles have been successfully synthesized through the chemical precipitation technique using nickel nitrate hexahydrate and ammonium carbonate. TGA results show a sharp weight loss at 350°C, caused by the conversion of nickel carbonate into nickel oxide. The results obtained from XRD and TEM confirms the nanocrystalline nature of the synthesized particles and the crystallite size was found to increase with increase in calcination temperatures. W-H analysis found that the micro-diffraction for NiO calcined at 400°C has large value, which decreases with increase in calcination temperature. UV-visible absorption studies revealed that an increase in the calcination temperature produces a blue shift in the absorption spectrum, and a decrease of band gap being a consequence of the increase in particle size. Also, photoluminescence studies showed that an increase in calcination temperature causes a decrease in PL intensity due to crystal growth. Furthermore, calcination temperature plays a vital role in controlling the particle size, which in turn helps to modify structural and optical properties of the formed NiO nanoparticles. Based on these systematic observations, it is concluded that NiO nanoparticles can be a promising material for optoelectronic applications because of its desired structural and optical properties.

Acknowledgements

Authors thank Nirmala College, Muvattupuzha for providing all the facilities to undertake this study. Authors are grateful to KSCSTE, Thiruvananthapuram, India for providing financial support. First author is thankful to U G C, New Delhi, India for providing financial grant under minor research project.

References

[1] Dharmaraj N., Prabu P., Nagarajan S., Kim C.H., Park J.H., Kim H.Y. Synthesis of nickel oxide nanoparticles using nickel acetate and poly(vinyl acetate) precursor. *Materials Science and Engineering B*, **128**, P. 111–114 (2006).

[2] Feldman C., Jungk H.O. Polyol-Mediated preparation of nanoscale oxide particles. *Angew Chem. Int. Ed.*, **40**, P. 359 (2001).

[3] Matsumiya M., Qiu F., et al. Thin-film Li-doped NiO for thermoelectric hydrogen gas sensor. *Thin Solid Films*, **419**(1-2), P. 213–217 (2002).

[4] Wang, Y., Zhu, J., et al. Preparation of NiO nanoparticles and their catalytic activity in the thermal decomposition of ammonium perchlorate. *Thermochim. Acta*, **437** (1–2), P. 106–109 (2005).

[5] Ichiyanagi Y., Wakabayashi N., et al. Magnetic properties of NiO nanoparticles. *Physica B*, **329–333** (Part 2), P. 862–863 (2003).

[6] Biju V., Abdul Khadar M. Analysis of AC electrical properties of nanocrystalline nickel oxide. *Mater. Sci. Eng. A*, **304–306**, P. 814–817 (2001).

[7] Li F., Chen H., Wang C., Hu K. A novel modified NiO cathode for molten carbonate fuel cells. *J. Electroanal. Chem.*, **531**(1), P. 53–60 (2002).

[8] Nuli Y., Zhao S., Qin Q. Nanocrystalline tin oxides and nickel oxide film anodes for Li-ion batteries. *J. Power Sources*, **114**(1), P. 113–120 (2003).

[9] Mallick P., Sahoo C. S., Mishra N. C. Structural and Optical Characterization of NiO nanoparticles synthesized by sol-gel route. *AIP Conf. Proc.*, **1461**, P. 229–232 (2012).

[10] Alagiri M., Ponnusamy S., Muthamizhchelvam C. Synthesis and Characterization of NiO nanoparticles by sol-gel method. *J. Mater Sci: mater Electron,* **23** P. 728–732 (2012).

[11] Jeevanandam P., Ranga Rao Pulimi V. Synthesis of nanocryst alline NiO by sol-gel and homogeneous precipitation methods. *Indian J Chem.*, **51**A, P. 586–590 (2012).

[12] Mallick P., Chandana rath, Biswal R., Mishra N. C. Structure and magnetic properti es of Fe doped NiO. *Indian J. Phys.*, **83**, P. 517 (2009).

[13] Takami S., Hayakawa R., Wakayama Y., Chikyow T. Continuous hydrothermal synthesis of nickel oxide nanoplates and their use as nanoinks for p-type channel material in a bottom-gate field-effect transistor. *Nanotechnol*, **21**, P. 134009 (2010).

[14] Anandan K., Rajendran V. Morphological and size effects of NiO nanoparticles via solvothermal process and their optical properties. *Mater. Sci. Semicond. Process*, **14**, P. 43 (2011).

[15] Chakrabarty S., Chatterjee K. Synthesis and characterization of nanodimensional NiO semiconductor. *J. Phy. Sci.*, **13**, P. 245–250 (2008).

[16] Jianfen Li, Rong Yan, et al. Preparation of nano-nio particles and evaluation of their catalytic activity in pyrolyzing biomass components. *American Chem. Soc.*, P. 1021 (2008).

[17] Jahromi S. P., Huang N. M., Muhamad M. R., Lim H. N. Solvothermal synthesis of SnO_2/graphene nanocomposites for supercapacitor application. *Ceram. Int.*, **39**, P. 3909 (2008).

[18] Varghese T., Balakrishna K. M. *Nanotechnology: An introduction to synthesis, properties and applications.* Atlantic Publishers, New Delhi, 2011, P. 111.

[19] Mote V.D., Purushotham Y., Dole B.N. Williamson-Hall analysis in estimation of lattice strain in nanometer-sized ZnO particles. *J. Theor Appl Phys.* **6**:1–8 (2012).

[20] Prabhu Y. T., Venkateswara K. R., Sesha V.S.K. and Siva Kumari B. X-ray analysis of Fe doped ZnO nanoparticles by Williamson-Hall and size-strain methods. *Int. J. Engg. Adv. Tech.*, **2**(4), P. 268 (2013).

[21] Williamson G.K. Hall W. H. X-ray line broadening from filed Al and W. *Acta Metall.*, **1**, P. 22 (1953).

[22] Fernández G. M., Martínez-Arias A., Hanson J. C., Rodríguez J. A. Nanostructured oxides in chemistry: Characterization and properties. *Chem. Rev.*, **104**, P. 4063 (2004).

[23] Di Monte R., Kašpar J. Nanostructured CeO_2-ZrO_2 mixed oxides. *Catal. Today*, **100**, P. 27 (2005).